



1 **Refined burned-area mapping protocol using Sentinel-2 data**
2 **increases estimate of 2019 Indonesian burning**

3 David L.A. Gaveau¹ Adria Descals², Mohammad A. Salim¹, Douglas Sheil³, Sean Sloan^{4,5}

4 ¹ TheTreeMap Bagadou Bas 46600 Martel, France

5 ² CREAM, Centre de Recerca Ecològica i Aplicacions Forestals, E08193 Bellaterra (Cerdanyola de Vallès),
6 Catalonia, Spain

7 ³ Forest Ecology and Forest Management Group, Wageningen University & Research, PO Box 47, 6700 AA,
8 Wageningen, The Netherlands

9 ⁴ Department of Geography, Vancouver Island University, Nanaimo, BC, Canada &

10 ⁵ Fenner School of Environment and Society, Australia National University, Canberra, ACT, Australia

11 Correspondence to: David Gaveau (d.gaveau@thetree.com)

12



13

14 **Abstract**

15 Like many tropical forest nations, Indonesia is challenged by landscape fires. A confident understanding of the
16 area and distribution of burning is crucial to understanding the implications of these fires and how they might best
17 be reduced. Given uncertainties surrounding different burned-area estimates, and the substantial differences that
18 arise using different approaches, the accuracy, and merits of such estimates require formal examination.

19 Despite investment in fire mitigation measures since the severe El-Niño 2015 fire season, severe burning struck
20 Indonesia again in late 2019. Here, drawing on Sentinel-2 satellite time-series analysis, we present and validate
21 new 2019 burned-area estimates for Indonesia. The corresponding burned-area map is available at:
22 <https://doi.org/10.5281/zenodo.4551243>. We show that >3.11 million hectares (Mha) burned in 2019, 31% of
23 which on peatlands. This burned-area extent is double the Landsat-derived Official estimate of 1.64 Mha from the
24 Indonesian Ministry of Environment and Forestry, and 50% more than the MODIS MCD64A1 burned-area
25 estimate of 2.03 Mha. It has greater reliability as these alternatives, attaining a user's accuracy of 97.9% (CI:
26 97.1%-98.8%) compared to 95.1% (CI: 93.5%-96.7%) and 76% (CI: 73.3%-78.7%), respectively. It omits fewer
27 burned areas, particularly smaller- (<100 ha) to intermediate-sized (1000 ha) burn scars, attaining a producer's
28 accuracy of 75.6% (CI: 68.3%-83.0%) compared to 49.5% (CI: 42.5%-56.6%) and 53.1% (CI: 45.8%-60.5%),
29 respectively. The frequency–area distribution of the Sentinel-2 burn scars follows the apparent fractal-like power-
30 law or “pareto” pattern often reported in other extensive fire studies, suggesting good detection over several
31 magnitudes of scale. Our relatively accurate estimates have important implications for carbon-emission
32 calculations from forest and peatland fires in Indonesia. Our approach is amenable to the ongoing production of
33 accurate annual burned-area maps for environmental monitoring and policy in South-East Asia.

34

35 **1. Introduction**

36 Landscape fires are a global concern due to their impacts. These impacts include wildlife habitat loss and
37 degradation, the associated emissions of greenhouse gases and toxic smoke, and the consequences for wildlife,
38 human health, transport, tourism, and economic activity across Southeast Asia. Fires, though scarce in wet forest
39 landscapes, have long been an element of traditional swidden agriculture and land clearance. Although the causes
40 and motivations of modern-day fire use can be complex (Dennis et al., 2005), many fires are lit by farmers and
41 companies when conditions permit to burn debris and enrich the soils before planting (Gaveau et al.,
42 2014;Adrianto et al., 2020) or to maintain existing agricultural land (paddy fields, farm fallow). The likelihood,
43 scale and intensity of such fires are greatly heightened during periods of anomalously low rainfall (Sloan et al.,
44 2017;Field et al., 2016), as fires readily spread uncontrolled beyond the intended areas (Gaveau et al., 2017),
45 largely over degraded lands (Miettinen et al., 2017;Lohberger et al., 2018) but also penetrate into forest near the
46 edge (Nikonovas et al., 2020). Intact rainforests don't burn without the prolonged droughts that favor the
47 accumulation of sufficient dry fuel, and while many live trees often remain (van Nieuwstadt and Sheil, 2005) the
48 resulting changes to forest structure increase the likelihood of further fires (Nikonovas et al., 2020;Cochrane,
49 2003). In Indonesia, droughts are often associated with years when anomalously cold sea surface temperatures
50 surround Indonesia and warm waters develop in the eastern Pacific Ocean (El Niño Southern Oscillation, ENSO)
51 and in the western Indian Ocean (Positive Indian Ocean Dipole, IOD+) (Field et al., 2009), although short, but



52 intense, fire episodes can also occur during climatically-normal years, or under Julian Madden weather conditions
53 (Gaveau et al., 2014;Koplitz et al., 2018). Austin et al. (2019) estimated that forest conversion to grasslands by
54 repeated fires accounted for 20% of total forest loss in Indonesia between 2001 and 2016.

55 The location, context, extent, and timing of fires have major implications for their impacts and their management.
56 During 2015, a strong El Niño year, fires burned an estimated 2.6-4.5 million hectares across Indonesia (Sipongi,
57 2020;Lohberger et al., 2018) and emitted 1.2 billion tons of CO₂ equivalent (or 884 million tons of CO₂) (Huijnen
58 et al., 2016), representing half of Indonesia’s total greenhouse gas emissions for that year (Gütschow et al., 2019).
59 In Palangkaraya, the capital city of Central Kalimantan province, daily average particulate matter (PM₁₀)
60 concentrations often reached 1000 to 3000 µg m⁻³ amongst the worst sustained air quality ever recorded worldwide
61 (Wooster et al., 2018). For reference, 50 µg m⁻³ is a short-term (24-h) exposure limit set by the World Health
62 Organization (WHO), and 300 µg m⁻³ is “extremely hazardous” according to by the Singapore National
63 Environment Agency. Over half a million people suffered respiratory problems in the aftermath, and between
64 12,000 and 100,000 premature deaths were estimated to result (Koplitz et al., 2016;Crippa et al., 2016). Although
65 2015 burning was approximately half as severe/extensive as 1997, the most severe El Niño and fire season on
66 record (Fanin and Werf, 2017), peatlands burned about 50% more extensively in 2015 (Fanin and Werf, 2017).
67 This pattern tracks a growing incidence of elevated peatland burning despite apparent long-term mitigation
68 (declines) to extreme fire activity (Sloan et al., Under Review).

69
70 In response to severe 2015 burning, the Indonesian government instituted several ambitious mitigation schemes.
71 Fire bans were enforced by dedicated command posts established in 731 fire-prone agricultural villages or *desas*
72 (~12 Mha), recently expanded to some 4000 village areas, with some apparent success in suppressing burning
73 (Sloan et al., Under Review). Simultaneously, in recognition that degraded peatlands are the primary source of
74 haze, the government pursued a new peatland restoration agenda. The Peatland Restoration Agency or *Badan*
75 *Restorasi Gambut* (BRG) was established in 2016 and declared a 2.67 Mha peatland-restoration target across 7
76 provinces host to >70% of the national burned area (Kalimantan Barat, Kalimantan Tengah and Kalimantan
77 Selatan, Papua, Jambi, Riau, and Sumatra Selatan). The seven provinces are largely the same as those actively
78 enforcing targeted fire bans. Restoration and fire-suppression initiatives driven by pulp-and-paper and agro-
79 industrial companies severely impacted by fire also flourished (Carmenta et al., 2020). These companies are
80 mandated to actively restore some of the targeted-for-restoration degraded peatlands (2.67 Mha).

81
82 Despite the investment in these measures since 2015, and some initial success, severe burning struck Indonesia
83 again in late 2019. This time a positive Indian Ocean Dipole event, rather than an ENSO weather system, was
84 responsible for widespread droughts, although the changing nature of these relationships and other weather
85 phenomenon remain a subject of ongoing research (Kurniadi et al., 2021;Cai et al., 2021). While Sloan et al.
86 (Under Review) suggest that 2019 fire activity was lower than might have occurred under the conditions
87 otherwise, the total number of MODIS active-fire detections in late 2019 was still amongst the greatest recorded
88 since 2001 in the village areas targeted for fire suppression, excepting 2015 (Sloan et al., Under Review).
89 However, counts of active-fire detections are not the same as estimates of area burned (Tansey et al., 2008) and
90 for 2019 such area estimates remain uncertain.

91
92 Accurate estimates of burned lands, and in particular assessments of peat fires, are key to ambitious Indonesian
93 climate-change atmospheric carbon (C) reduction national commitments (DGCC, 2019). Burned-area estimates



94 are used to calculate annual C emissions from fires, contribute to forensic analyses in landholdings (e.g. oil palm
95 and pulp & paper concessions), and help identify the result of policies and practices intended to reduce or control
96 fires, such as land enforcement and restoration of degraded lands.

97

98 Using visual interpretations of time-series Landsat-8 imagery, the Indonesian Ministry of Environment and
99 Forestry (MOEF) estimated that 1.64 Mha burned in 2019 (Sipongi, 2020). The commonly used global MODIS
100 annual burned-area product (MCD64A1, collection 6) (Giglio et al., 2018) indicated 2.01 Mha burning in 2019.
101 Both datasets suffer shortcomings that bias their estimates, however. The coarse 500-m spatial resolution
102 MCD64A1 data omit smaller fires and thus overlook many localized events and overestimate larger ones. The
103 MCD64A1 dataset reports omission and commission errors of 40% and 22% globally for the ‘burned’ class
104 (Giglio et al., 2018). This validation is based on independent globally distributed visually interpreted reference
105 satellite data, however none over Indonesia. Conversely, the Landsat imagery underlying MOEF estimates
106 (hereafter ‘Official estimate’) are, while finer scale, observed every 16 days at best (typically much less due to
107 cloud and smoke), meaning that many burn scars may remain undetected. Also, smaller-scale and/or dispersed
108 fire activity may be underestimated, considering the challenges of their visual interpretation and delineation. A
109 thorough accuracy assessment is also not available for the official burned-area product. Given the unknown errors
110 around burned-area estimates, and the differences between them, the accuracy, and merits of the different mapping
111 approaches over Indonesia require formal examination.

112

113 Here, we present new and validated 2019 burned-area estimates for Indonesia using a time-series of the
114 atmospherically corrected surface reflectance multispectral images (level 2A product) taken by the Sentinel-2 A
115 and B satellites. With higher spatial resolution (20-m) and more frequent observations (5-day revisit time), the
116 Sentinel-2A and B satellites offer relatively comprehensive and accurate burned-area mapping (Huang et al.,
117 2016). As detailed below, we developed our method using the Google Earth Engine (Gorelick et al., 2017), in turn
118 allowing for its reproduction for ongoing burned-area monitoring. We also developed an independent reference
119 dataset to compare the accuracy of our estimate against the Official and MCD64A1 burned-area maps. Given the
120 lack of randomly distributed ground verifications of ‘burned’ and ‘unburned’ locations, we sought an efficient
121 way to extract reference sites by visually detecting either a smoke plume, a burn scar, or a heat source (flaming
122 front, or hotspot) from the archive of original time series Sentinel-2 images. Finally, we examine differences in
123 terms of scar-size frequency distributions among these three burned-area estimates to examine spatial patterns.

124

125 **2. Methods**

126 *2.1. Summary of methods*

127 A burned area is an area of land characterized by deposits of char and ash, and by alteration of vegetation cover
128 and structure. We mapped burned areas using a change -detection approach, i.e. by comparing Sentinel-2 infrared
129 signals recorded before and after a burning event (Liu et al., 2020). We assembled two national composite images
130 depicting vegetation condition before and after 2019 burning (Figure 1) by automatically extracting pairs of
131 nominally ‘burned’ and ‘unburned’ pixels from 47,220 original Sentinel-2 images acquired between 01 November
132 2018 and 31 December 2019. This reconstructed pair of pre- and post-fire images spans the entire 2019 burning
133 season. It is a convenient way to capture the entire burned landscape stored in just two image files. Subsequent to
134 the production of this image pair, we classified pixels of the pair as ‘burned’ or ‘unburned’ using a Random Forest



135 classification model trained on visually-identified pairs of pre- and post-fire pixels. Third, three independent
136 interpreters assembled a reference dataset by visually interpreting burn scars in the original time-series (5-day
137 repeat pass) Sentinel-2 images. Fourth and finally, we assessed our burned-area map, as well as the Official and
138 MCD64A1 burned-area maps, against our reference dataset to gauge the reliability and accuracy of the three
139 burned-areas products. Finally, we tested whether, and how, the three burned-area estimates differed in their
140 tendencies to incorporate burn scars of larger or smaller sizes.

141

142 *2.2. Pre- and post-fire Sentinel-2 national composite images of 2019*

143 Here, we describe our automated procedure to extract pairs of ‘burned’ and ‘unburned’ pixels from 47,220
144 Sentinel-2 images acquired throughout 2019. This set of pixel pairs was used to create the national composite pre-
145 and post-fire images and guide subsequent supervised classifications of burned areas nationally. Prior to running
146 this procedure, we removed cloud-impacted pixels using the Sentinel-2 imagery quality flag (this flag provides
147 information about clouds, cloud shadows, and other non-valid observations) produced by the ATCOR algorithm
148 and included in the atmospherically-corrected surface reflectance multispectral images of the Sentinel-2 A and B
149 satellites Surface Reflectance products (Level 2A product) (Fletcher, 2012).

150 A time series of the Normalized Burned Ratio (NBR), given as $(\text{NIR}-\text{SWIR}) / (\text{NIR}+\text{SWIR})$, represents a
151 convenient index to detect if and when a disturbance in the vegetation occurred in 2019, such as a burning
152 event (Key and Benson, 1999). Before a fire, vegetated pixels register high NBR values close to 1 because
153 reflectance in near-infrared spectrum (NIR; wavelength=0.842 μm ; Band 8) is high due to the chlorophyll content
154 of the vegetation (open circles before fire in Figure 2). The NBR of burned vegetation typically declines due to
155 chlorophyll and leaf destruction, such that NBR of ≤ 0 are apparent for a few weeks after a fire, while the
156 reflectance of short-wave-infrared spectrum (SWIR; wavelength = 1.610 μm or 2.190 μm ; Band 11 or Band 12)
157 increases due to charred material and exposed ground cover. We analyzed a NBR time series for approximately
158 94.5 billion 400 m² pixel pairs (Indonesia’s landmass =198 Mha) to detect the day when a pixel’s vegetation was
159 disturbed by fire.

160 We detected breaks in NBR time series with a moving-window approach. Every two days, a moving window
161 scanned NBR values three months prior and one month after the central day of the window. The output value of
162 the moving window (blue dots in Figure 2) is the difference between average NBR values observed before and
163 after the central day. The day of the year when this difference reached a maximum corresponded to the moment
164 NBR dropped most markedly in each pixel over a two-day period, flagging a disturbance to the pixel’s vegetation
165 potentially caused by fire. At this date, we created a pair of pre- and post-fire pixels by selecting the median Red,
166 NIR and SWIR spectral values acquired three months before and one month after the potential burning event. We
167 selected a one-month window rather than a three-month window to compute the post-fire image to maximize our
168 chances to detect a fresh burn scar, given that burned areas on degraded lands and savanna tend to re-green rapidly.

169 *2.3. Supervised burned/unburned classification.*

170 We used the Random Forest supervised classification algorithm (Breiman, 2001), available via the Google Earth
171 Engine, to classify burned areas from the pair of pre- and post-fire image composites created above. Supervised
172 classifiers require ‘training data’, that is, exemplary spectral signatures of ‘burned’ and ‘unburned’ lands in the
173 present case, to guide the algorithm to reliably classify the target classes. The spectral signatures (i.e., the
174 reflectance values in the pre- and post-fire composite images) are the predictive variables of the classification



175 model. We used the NBR and all available Sentinel-2 spectral bands of the pre- and post-fire image composites
176 as input to the Random Forest model.

177 We trained the Random Forest algorithm using 988 training pixels, being point coordinates labelled as either
178 ‘burned’ (317 points) or as ‘unburned’ (671 points). The selection of these pixels was realized by visual
179 interpretation of the pre- and post- fire image composites. Burned areas show a distinctive dark (low albedo)
180 brown/red color in the SWIR-NIR-Red composite image when displayed as Red-Green-Blue channels (Figure 1).
181 The training pixels were collected in a variety of landcover types to ensure the representativeness of the training
182 dataset and the satisfactory generalization of the classification model across Indonesia. We selected training pixels
183 focused explicitly on medium-to-high burn severity, i.e. areas where the distinctive red color in the SWIR-NIR-
184 Red composite image looked the darkest, indicating that all or most of the vegetation/soil burned. This aspect of
185 the methodology hedged against over-estimation of total burned area by minimizing so-called “false positives”.
186 It may however exclude areas with implied low-burn severity, such as understory fires (below an intact forest
187 canopy) and even some agricultural and grassland fires. By prioritizing confident identification of fires over
188 absolute burned-area coverage, as well as by duly validating our estimates, this conservative approach has the
189 advantage of assuaging sensitivities concerning false positives (Rochmyaningsih, 2020).

190

191 2.4. Burned-area map validation.

192 The Gold standard is to validate the map against a sufficiently large reference dataset developed based on ground
193 visits to ‘burned’ and ‘unburned’ sites sampled randomly across the country (Olofsson et al. 2014). We sought
194 another way to generate the reference dataset because the sample of GPS locations of ‘burned’ locations collected
195 by Indonesian government were not available. Given the laborious scale of this validation exercise, we validated
196 our burned-area estimates for only the seven provinces prioritized by the Indonesian Government for restoration
197 of fire-prone degraded lands (Kalimantan Barat, Kalimantan Tengah and Kalimantan Selatan, Papua, Jambi, Riau,
198 and Sumatra Selatan). These provinces are also those that typically burn most extensively. We used visual
199 interpretations of the original time-series Sentinel-2 imagery acquired every 5 days over 2019 at 1298 randomly
200 selected sites (one site = one pixel of 20 m x 20 m) to detect flaming fronts (fire hotspots) and other signs of
201 burning (smoke and charred vegetation). We used these reference data to calculate the overall accuracy (OA),
202 producer’s accuracy (PA), and user’s accuracy (UA) with a 95% confidence interval, of all three burned area maps
203 (i.e., our Sentinel-derived burned-area classification, the official Landsat-based burned-area map, and the
204 MCD64A1 product) following “good practices” for estimating area and assessing accuracy reported by Olofsson
205 et al. 2014. We use the term ‘*mapped burned-area*’ for the area classified as burned by each burned-area map.
206 We employ the term ‘*corrected burned-area*’ for the estimation of the burned area based on the validation of a
207 given burned-area map against the reference dataset, following the practices in Olofsson et al. 2014. For instance,
208 a high omission rate in the ‘burned’ class of a given burned-area estimate would potentially lead to a lower *mapped*
209 *area* than a *corrected area* for that estimate, while a high commission rate would potentially lead to a higher
210 *mapped area* than the *corrected area*. The *corrected area* represents an estimation of the actual burned area for
211 year 2019 computed for each of the three datasets separately. The accuracy of the burned area map, and the sample
212 size of the reference dataset, play a role in the confidence interval of *corrected area* estimate. Lower map accuracy
213 and smaller sample size mean wider confidence intervals.

214



215 2.4.1. *Reference site sampling design*

216 The good practices for estimating area and assessing accuracy reported in Olofsson et al. 2014 assume a simple
217 random sampling or a stratified random sampling in the generation of the reference dataset. In our case study, we
218 employed a stratified-random sampling approach to ensure an acceptable sample of ‘burned’ reference sites. Our
219 stratified approach was necessary given that the ‘burned’ class was rare over the study area: the area of seven
220 provinces of interest is 87.6 Mha and the combined area detected as burned by all three datasets represented only
221 3.1% of this area.

222 For the generation of the 1298 reference sites, we first randomly sampled (i) 419 sites across from the areas
223 classified ‘burned’ by the three datasets (red area in Figure 3a; Supplementary Table S1), and (ii) 879 sites in
224 areas classified as ‘unburned’ by all three datasets hereafter denoted U (grey area in Figure 3a). This sample size
225 is deemed sufficient and comparable to other map assessments at larger scale (Stehman et al., 2003;Olofsson et
226 al., 2014).

227 This initial sample of 1298 total sites present a shortcoming for direct pair-wise comparisons of between the
228 reference dataset and each of the three burned-area maps individually. Specifically, sampling densities in the
229 reference dataset were far greater in areas classified ‘burned’ by the three datasets (red area in Figure 3a) compared
230 to the area deemed ‘unburned’ by all three datasets, hereafter denoted U (grey area in Figure 3a). Consequently,
231 for the validation of a given burned-area dataset, its total number of ‘unburned’ reference sites would be over-
232 sampled upon defining ‘unburned’ reference sites with reference to U as well as areas classified as burned uniquely
233 by one of the other two maps (cyan areas in Figure 3b, c, d, hereafter denoted as U’). Such over-sampling of
234 reference sites in the realm of U’ would violate the stratified-sampling approach described in Olofsson et al.
235 (2014) and would lead to an erroneous accuracy assessment. In order to achieve a balanced stratified sampling of
236 reference sites across ‘burned’ and ‘unburned’ areas of each dataset, we generated three subsamples from the
237 initial 1298 reference sites (red areas in Figures 4f,g,h) and used these subsamples to validate each dataset. These
238 three subsamples were generated by randomly excluding reference sites from the realm of U’ in Figure 3b, c and
239 d, respectively, until the density of reference sites in U’ equaled the density of the larger unburned area U. For
240 instance, for the validation of the Official burned-area map, the density of reference sites in U was 10.36 sites/Mha,
241 and the extent of U’ was 1.551 Mha, such that the number of reference sites to retain in U’ for this validation was
242 given as $1.551 \text{ Mha} \times 10.36 \text{ sites/Mha} = 16$ sites. The calculations of the number of sites removed from each
243 subsample are illustrated in Supplementary Table S2. The final, adjusted, stratified subsamples of reference sites
244 used for validation is given in Table 1.

245

246

247

248

249

250



251 2.4.2. *Interpretation of the burned-area reference dataset*

252 We developed a series of scripts in the Google Earth Engine to streamline the visual interpretation of the reference
253 sites. Specifically, we adapted a script written by (Olofsson et al. 2014) to rapidly scan the time-series of original
254 Sentinel-2 images in visible and infrared bands and thus visually detect either a smoke plume, a burn scar, or a
255 heat source (flaming front), and determine whether and when in 2019 a reference site burned. The script enabled
256 the interpreter to interactively track the evolution of NBR values and patterns over the 2019 time series of 5-day
257 images. Reference sites were investigated for burning wherever a marked drop in the NBR time series was
258 detected, indicating a disturbance in the vegetation. For reference sites where a disturbed area was observed, we
259 subsequently reviewed the last few images before the drop in NBR and the first few images after the drop.
260 Interpreters looked for three distinct signs of burning in these images to confirm them as burned: (i) smoke plumes;
261 (ii) flaming fronts – that is, a line a moving fire where the combustion is primarily flaming; and (iii) rapid changes
262 in color from ‘green’ to ‘red’, characteristic of a transition to charred vegetation (Figure 4). If rapid changes in
263 color were observed over the reference site, with at least one direct feature (smoke or flame) in its vicinity, this
264 indicated a fresh burn scar, and the reference site was declared ‘burned’. If none of these three features were
265 observed, the reference site was declared ‘unburned’.

266

267

268 Three interpreters independently reviewed the time-series of images and associated NBR trends for all reference
269 sites (N=1298). To reduce uncertainties associated with the interpretation of the imagery, the results of the three
270 interpreters were compared to each other. If all three interpreters recorded the same interpretation and timing of a
271 burning event for a given reference site, their interpretations were retained. If one or more interpreters disagreed,
272 all interpreters reviewed the data and resolved discrepancies by consensus. In some cases, it was difficult to
273 reconcile disagreements because of poor image quality or because of uncertain spectral patterns. Therefore, if
274 possible, interpreters also explored other satellite images (e.g. Landsat) to detect the presence of fire and resolve
275 disagreements for a given reference site. The sites in which the three interpreters disagreed were ultimately
276 excluded (70 sites) from the reference dataset. For these excluded sites, disagreement typically resulted from
277 uncertainties over the boundary of burned or unburned areas, or because the imagery was not clear enough. The
278 final sample size explored here, N=1298, excludes the discarded points of disagreement in question.

279 We created a second script to generate snapshot images (see examples in Figure 4) depicting infrared spectral
280 conditions, shortly before and shortly after a fire, as well as the corresponding image dates. Interpreters recorded
281 and geotagged a snapshot of before and after fire condition at every reference site (for which a burned area was
282 detected) to enable third-party reviewers to check the consistency and validity of interpretations on site-by-site
283 basis (See Data Availability).

284

285 2.4.3. *Burn scar size comparisons.*

286 We tested whether, and how, the three burned-area estimates differed in their tendencies to incorporate burn scars
287 of larger or smaller sizes. Specifically, we compared the frequency distributions of burn-scar size amongst the
288 three estimates to test for similarity and qualify any distinguishing differences on the part of our Sentinel-based
289 estimate. Differences amongst burn-scar size frequency distributions implies that a given burned-area estimate is
290 more or less inclusive of burn scars of a given size, regardless of absolute differences to total burned area between



291 the estimates. Inter-estimate comparisons of burn-scar size frequency is analogous to tests of whether the
292 ‘samples’ of burn scars defined by each estimate describe the same, ultimately partially-observed universe of fire
293 activity. Significant inter-estimate differences imply greater or lesser inclusion of a given realm of fire activity –
294 e.g., small-scale agricultural burning, plantation fires, extreme wildfires – thus indicating bias (or lack thereof)
295 without defining such realms explicitly.

296 For all three estimates, we employed the Kruskal-Wallis H test of differences with respect to the ‘location’ of
297 frequency distributions along a continuum of burn-scar sizes. Given significant inter-estimate differences
298 according to this three-way test, we tested for two-way differences in the shape and location of the scar-size
299 frequency distribution (Kolmogorov-Smirnov test), as well as two-way differences in medians (Mann-Whitney U
300 test), between our Sentinel estimate and either the Official or MODIS estimate individually. We performed all
301 comparisons for scar-size cohorts > 6.25 ha, > 20 ha, > 100 ha, > 1000 ha, and > 5000 ha, without Bonferonni
302 correction given the nested nature of these cohorts. Testing for similarity over increasingly large scar-size cohorts
303 clarified the degree to which significant inter-estimate differences were attributable to the inclusion or omission
304 of a given cohort.

305

306 We excluded scars <6.25 ha because this is the minimum observable burn scar size according to MODIS data,
307 given pixel resolution, and it is already evident that our Sentinel estimates are distinguished by their ability to
308 detect burn scars below this threshold. The Landsat-8 Official estimates similarly have few scars < 6.25 ha due
309 to the challenging nature of visual interpretations at such fine scales. In relation to Sentinel and MODIS estimates,
310 for which burned areas were originally mapped as arrays of pixels, we defined a burn scar to be any array of pixels
311 contiguous across cardinal directions but not diagonals. For the Official estimate, burn scars are as manually
312 delineated via visual interpretation by interpreters from the Government of Indonesia. All scars are spatially and
313 temporally discrete, such that scars of a given estimate that overlap spatially but not temporally are considered
314 separate.

315

316 **3. Results**

317

318 *3.2. Increased Burned-Area Estimates*

319 Our Indonesia-wide burned-area estimate, based on the classification of the pair of pre- and post-fire Sentinel-2
320 composites, are larger than the Official estimates as well as the MODIS MCD64A1 to a lesser degree. We estimate
321 3.11 million hectares (Mha) burned in 2019 across Indonesia, of which 31% were on peat (Figure 5). The extent
322 of peatlands were defined using a national dataset from the Ministry of Agriculture (Ritung et al., 2011). In
323 contrast, Official burned-area estimates, based on visual interpretation of Landsat-8 imagery, report only about
324 half as much burned area, at 1.64 Mha, of which 39% was on peat. Our estimates are similarly considerably
325 greater than the MODIS MCD64A1 product, which reports 2.04 Mha burned in 2019, or two-thirds of our
326 estimate, with 40% on peat. The greater burning extent and proportionally lesser extent of peatland burning
327 according to our estimates suggest that our estimates are particularly more inclusive of burning across mineral
328 soils.

329



330 In the seven provinces for which we carried out the accuracy assessment, our Sentinel-2 estimates and the Official
331 Landsat-8 estimates both report excellent user's accuracies (UA) for the 'burned' class, at 97.9% (CI: 97.1%-
332 98.8%) and 95.1% (CI: 93.5%-96.7%) respectively, indicating a mere 2.9%-4.9% commission-error rate (Table
333 2, Supplementary Table S3). The producer's accuracies (PA) are comparatively lower for both datasets, but
334 notably less so for our estimates, at 75.6% (CI: 68.3%-83.0%) and 49.5% (CI: 42.5%-56.6%) for our estimate and
335 the Official dataset, respectively. In other words, for any burned area in our reference dataset, there is a 75.6%
336 chance that it will be correctly mapped as burned by our estimate, compared to only a 49.5% for the official
337 estimate. This is in keeping with the greater tendency of the Sentinel-2 estimate to capture more smaller and
338 intermediate-size burn scars. The MCD64A1 data had a much lower UA for the burned class, at 76.0% (CI:
339 73.3%-78.7%), as well as a much lower and a PA for the burned class, at 53.1% (CI: 45.8%-60.5%), qualifying it
340 as the least reliable and accurate of the three estimates notwithstanding comparable high overall accuracy (Table
341 2).

342 All three burned-area maps underestimate the true burned area extent, as per their respective PA figures, but our
343 Sentinel-based map underestimates considerably less severely without a corresponding loss of user's accuracy.
344 The corrected burned area of the seven provinces is higher than the mapped area for all the three burned area
345 maps. Again, however, our Sentinel-based map area most closely approximates its corresponding corrected burned
346 area (Table 2). Whereas our Sentinel-based mapped burned area indicates that 1.84 Mha burned in the seven
347 provinces (or 59% of our total national estimated burned area), the corrected burned area is 2.38 Mha (CI: 2.14
348 Mha-2.61 Mha) (Table 2), for a discrepancy of 0.54 Mha. In contrast, the official estimate indicates 1.19 Mha
349 burned in the seven provinces (73% of its corresponding total), and a corrected burned area of 2.29 Mha (CI: 1.96
350 Mha-2.63 Mha), for a 1.1 Mha discrepancy. Likewise, the MCD64A1 dataset mapped 1.58 Mha burned in the
351 seven provinces and has a corrected burned area of 2.27 Mha (CI: 1.94 Mha-2.59 Mha), for a 0.69 Mha
352 discrepancy. Although, we cannot extrapolate a corrected burned area across Indonesia, we confidently conclude
353 that appreciably more than 3.11 Mha burned nationally in 2019.

354 *3.1. Burn scar size comparison.*

355 The Sentinel, Official and MCD64A1 estimates captured significantly distinct realms of fire activity, as
356 represented by their relative frequencies of scar sizes (Figure S2). The three estimates differ from one another
357 decreasingly over increasingly larger minimum scar-size thresholds, however, and are statistically
358 indistinguishable for scars > 5000 ha indicative of extreme fire activity (Table 3). In other words, all three
359 estimates capture very large scars (>5000 ha) equally well, and distinctions amongst the estimates concentrate
360 amongst small (<100 ha), intermediate (100-1000 ha) and larger (1000-5000 ha) scars, in decreasing order of
361 degree as indicated by the magnitude of the test statistics in Table 3.

362

363

364 Inclusivity of smaller and intermediate scars is the primary source of difference among estimates. Compared to
365 Official or MCD64A1 estimates, the Sentinel estimate has a significantly greater relative frequency of small scars
366 (< 100 ha), especially amongst the smallest of these scars (Table 4). This is indicative of a greater detection of
367 the realm of fire activity presumably characterized by small-scale agriculture fires and similar, small-scale
368 controlled burning. The Sentinel estimate similarly has a greater relative frequency of intermediate scars (100-
369 1000 ha), but less acutely so, with inter-estimate differences being more moderate for the Official estimate than



370 the MCD64A1 estimate (Table 4, Figure 6 Figure S2). For scars >1000 ha, the Sentinel estimate differs only
371 relative to the official estimate (Table 3), seemingly due to the latter's lesser estimation of large and very large
372 scars (Figure 6). Note for instance the increasingly large divergence between the cumulative burned-area curves
373 for the Sentinel-2 and the Official estimates in Figure 6 for scars > 1000 ha. For very large scars (> 5000 ha),
374 two-way comparisons in Table 4 again report no significant statistical differences in burn-scar detection rates
375 between the Sentinel and alternative estimates. However, given the small sample of patches > 5000 ha, it is
376 noteworthy that the Sentinel estimate captures more very large scars compared to Official estimates (n=56 vs
377 n=16) and avoids critical omissions made by both Official or MCD64A1 estimates for extremely large scars
378 (>15,000 ha) on peatlands around Berbak National Park in Jambi Province, Sumatra (Figure 1, Inset A).

379

380 In summary, the greater overall burned-area estimate of our Sentinel data compared to the Official and MCD64A1
381 alternatives is largely attributable to differences in the inclusion of smaller and intermediately sized scars. Indeed,
382 the aerial sum of all Sentinel burn scars that are individually <~860 ha equals the entirety of the official burned-
383 area estimate (Figure 6). While the finer spatial resolution of Sentinel data must account for some of the inter-
384 estimate discrepancies, particularly relative to the MCD64A1 estimate and scars < 100 ha (Figure S2), overall the
385 discrepancies above seem more in keeping with our estimate's greater sensitivity to otherwise overlooked smaller-
386 scale burning. Hence, the inter-estimate differences qualify our Sentinel estimates not simply as more extensive
387 but also as qualitatively distinct in terms of the degree to which different realms of fire activity are captured. The
388 near linear log-log frequency–area distribution over several orders of scar-size of our Sentinel product indicates a
389 characteristic power-law relationship (Figure 6).

390 4. Discussion

391 We developed a method that generates two national composite Sentinel-2 images depicting vegetation condition
392 before and after burning in 2019 (Figure 1), and then classified this pair to extract burned areas using a Random
393 Forest supervised classification algorithm. We developed a comprehensive validation protocol to strictly assess
394 the reliability and accuracy of our product based on visual interpretation of dense time-series Sentinel-2 original
395 images, and also applied this validation to the widely used global MODIS burned-area product (MCD64A1,
396 collection 6) (Giglio et al., 2018) and to the Official burned-area product of the Indonesian Ministry of
397 Environment and Forestry (MOEF) (Sipongi, 2020).

398 Our estimate is the most reliable and accurate and therefore captures more of the 2019 total burned area,
399 confirming that 20-m Sentinel-2 imagery is better suited to widespread small-scale agricultural burning in
400 Indonesia (Huang et al., 2016), while it also captures large burn scars relatively thoroughly. The study finds similar
401 omission and commission errors (47% and 24%) for the 'burned' class of MCD64A1 product as those presented
402 globally (40% and 22%) (Giglio et al., 2018). The underestimation of total burned area according to the
403 MCD64A1 product compared with our Sentinel-2 estimate is unsurprising, considering that the MODIS 500-m
404 pixel resolution struggles to detect smaller fires (Giglio et al., 2018). More surprising is the near 2:1 ratio by
405 which the Sentinel-2 estimates surpass the Landsat-8 Official estimate. Our examination shows that this
406 difference reflects differential detection of small- (<100 ha) to intermediate-sized (<1000 ha) burn scars.

407 The burn-scar frequency distribution of the Sentinel-2 estimate is characteristic of robust power-law relation
408 (Figure 6), a pattern typical of large scale fire studies (Malamud et al., 1998). Modern studies suggest that these
409 fractal-like patterns are often subtly more complex and can arise through a range of phenomena (Karsai et al.,



410 2020;Falk et al., 2007). We note that the Sentinel-2 estimate exhibits a size-frequency pattern that approximates
411 the linear expectation of a near scale-free power-law, or pareto distribution, compared to either of the alternative
412 burned-area estimates, both of which show a clearly S-shaped curve with less area at smaller and larger sizes,
413 indicating the bias by omission. These results, with different frequency patterns arising from burns from the same
414 regions in the same period, also highlight the danger in interpreting apparent burned-area patterns without careful
415 consideration of the limitations and biases that arise from the methods used to map them—an issue that may not
416 have always been sufficiently recognized in past assessments or policy.

417 Although both Sentinel-2 and Landsat-8 both observe the infrared wavelengths required to detect charred
418 vegetation and have similar spatial resolutions (20 m x 20 m and 30 m x 30 m, respectively), Sentinel-2 detects
419 more burns of the greater frequency of its coverage (five- versus sixteen-day revisit time). Also, our method
420 avails of the massive computational capabilities and automation of the Google Earth Engine, allowing us to
421 analyze more images and thus map more and smaller burn scars and associated details than could even the most
422 well-equipped team of visual interpreters.

423 Despite high reliability that every burn scar detected on the map was valid (2.9% commission error rate), our
424 method suffered a 24.4% omission error rate (burned areas that remained undetected). These rates reflect
425 necessary tradeoffs between commission and omission error in a context where conservative estimates are much
426 preferred for environmental policy and monitoring. We prioritized a low commission error rate (i.e. high user's
427 accuracy) over absolute burned-area coverage to address sensitivities (Rochmyaningsih, 2020). By hedging
428 against commission errors, our approach omitted hard-to-detect events, including low-intensity burns, such as
429 those that occur beneath the forest canopy on mineral soils (van Nieuwstadt and Sheil, 2005) or on savanna
430 grasslands, which tend to re-green rapidly. While further work is required to clarify and refine the optimal levels
431 of inclusivity and reliability, we emphasize that the production of before and after fire annual composite images
432 is relatively straightforward for the user community, given the availability of both the necessary imagery and our
433 Google Earth Scripts.

434 Sometimes commentators raise doubts about our ability to confidently estimate burn scars without extensive and
435 costly on-the-ground ground-truthing. Modern high-resolution remote sensing makes such on-the-ground checks
436 less essential than in the past as burned areas are readily identified with good accuracy in modern high-resolution
437 imagery such as that we used for our validation. The protocol developed here to generate a reference dataset based
438 on visual inspection of dense (5-day revisit time) satellite imagery is better suited than ground verifications of
439 'burned' and 'unburned' locations, because it allows the generation of extensive randomly-distributed well
440 characterised reference sites, a process too time-consuming and costly with field visits. The identification and
441 quantification of less-readily-detected burned areas, such as those under a closed forest canopy, remain a challenge
442 but will require dedicated and targeted research and would not be solved by ground-checks alone.

443 Accurate estimates of burned lands, in particular on peat, are central to address concerns about regional air quality,
444 and to ambitious national climate-change atmospheric carbon reduction commitments heavily reliant on improved
445 land/fire management (DGCC, 2019). Though we observed proportionally less peatland burning than the
446 alternative burned-area estimates (31% versus 39% and 40% for the Official and MCD64A1 products,
447 respectively), due to our more complete coverage, we observed more peatland burning absolutely (0.96 Mha) than
448 the official estimate (0.64 Mha). Given this large discrepancy for peatland burning, we anticipate that our
449 improved mapping approach will become a "gold-standard" reference to calculate carbon emissions from the 2019



450 fires in Indonesia. Combined with daily fire hotspots detected using thermal remote sensing, our detailed burned-
451 area map can help identify ignition sites and estimate fire duration more precisely, and therefore contribute to
452 forensic analyses of burning across landholdings (e.g. concession owners) as well as assess policies and practices
453 intended to reduce or control ignition events and the scale of fires (Watts et al., 2019).

454 The Indonesian government has shown some success in reducing fires (Sloan et al., in review). Apparent
455 reductions to fire activity would however ideally be qualified using our more inclusive and accurate burned-area
456 estimates. Further, the Indonesian government must also develop improved protocols to quantify the resulting
457 carbon emissions (DGCC, 2019). Our protocols for creating reliable and accurate burned area maps are replicable.
458 To further the adoption and reproduction of our approach, we have published all our protocols, scripts,
459 applications, burned-area map, reference data, pre-fire and post-fire Sentinel-2 composite images, and various
460 other outputs so that anyone may employ and revise them as they wish (see Data Availability).

461

462 **5. Code availability**

463 The code that generates the Sentinel-2 pre- and post-fire composites can be found at:
464 https://github.com/thetremap/IDN_annual_burned_area_detection

465 **6. Data Availability**

466 All the data including pre- and post-fire composites, all three burned area products, and reference points with
467 screenshots can be visualized online at this application portal:
468 <https://thetremap.users.earthengine.app/view/burn-area-validation-simplified>

469 The Sentinel-based burned area map and reference dataset are freely available for download at:
470 <https://doi.org/10.5281/zenodo.4551243>.

471 The dataset *2019_burnedarea_indonesia.shp* contains the 2019 burned-area estimates that we developed for
472 Indonesia using 20 m x 20 m time-series Sentinel-2 imagery. The reference dataset *Reference_dataset.shp*
473 contains 1298 reference points that we assembled and used to validate all three burned area products described in
474 this study. Each reference point includes attribute 'REFERENCE' to describe the values obtained by visual
475 interpretation: either 'NO' unburned or 'YES' burned. Each reference point has three attributes: 'C_SENTINEL'
476 'C_OFFICIAL' and 'C_MCD64A1' to describe the values of the classification of each burned area product: either
477 'NO' unburned or 'YES' burned. Finally, each reference point has three additional attributes: 'SENTINEL',
478 'OFFICIAL', and 'MCD64A1' to describe which burned area product this reference point validates. The values
479 are either 0: not validate or 1: validate.

480 The MODIS MCD64A1 dataset was obtained at: [https://developers.google.com/earth-](https://developers.google.com/earth-engine/datasets/catalog/MODIS_006_MCD64A1)
481 [engine/datasets/catalog/MODIS_006_MCD64A1](https://developers.google.com/earth-engine/datasets/catalog/MODIS_006_MCD64A1). The official burned area dataset from the Ministry of
482 Environment and Forestry (MOEF) was obtained at: <https://geoportal.menlhk.go.id/webgis/index.php/en/>

483 The Sentinel-2 Level 2A used in this study are available at <https://scihub.copernicus.eu/> and can be retrieved in
484 Google Earth Engine. The Sentinel- 2 data are hosted and accessed in the Earth Engine data catalog (the links to
485 the data are https://developers.google.com/earth-engine/datasets/catalog/COPERNICUS_S2_SR). Data ingested
486 and hosted in Google Earth Engine are always maintained in their original projection, resolution, and bit depth
487 (Gorelick et al., 2017).



488

489 **Financial support.** Funding by the CGIAR Research Program on Forests, Trees and Agroforestry (CRP-FTA),
490 with financial support from the donors to the CGIAR Fund, is recognized.

491

492 **Author Contributions.** D.L.A.G. designed the study. D.L.A.G, M.A.S. and A.D designed the burn scar detection
493 method. M.A.S. and A.D wrote the code in Google Earth Engine. D.L.A.G, M.A.S. and A.D. carried out the
494 validation. S.S. carried out the burn scar size analysis. D.L.A.G., A.D. S.S. and D.S. interpreted the results and
495 wrote the manuscript and produced the figures.

496

497 **Competing interests.** The authors declare no competing interests. Readers are welcome to comment on the online
498 version of the paper.

499

500 **References**

501 Adrianto, H. A., Spracklen, D. V., Arnold, S. R., Sitanggang, I. S., and Syaufina, L.: Forest and Land Fires Are
502 Mainly Associated with Deforestation in Riau Province, Indonesia, *Remote Sensing*, 12, 3, 2020.

503

504 Breiman, L.: Random forests, *Machine learning*, 45, 5-32, 2001.

505

506 Cai, W., Yang, K., Wu, L., Huang, G., Santoso, A., Ng, B., Wang, G., and Yamagata, T.: Opposite response of
507 strong and moderate positive Indian Ocean Dipole to global warming, *Nature Climate Change*, 11, 27-32,
508 10.1038/s41558-020-00943-1, 2021.

509

510 Carmenta, R., Zabala, A., Trihadmojo, B., Gaveau, D., Salim, M. A., and Phelps, J.: Evaluating bundles of
511 interventions to prevent peat-fires in Indonesia, *Global Environmental Change*, 102154, 2020.

512

513 Cochran, M. A.: Fire science for rainforests, *Nature*, 421, 913-919, 2003.

514

515 Crippa, P., Castruccio, S., Archer-Nicholls, S., Lebron, G., Kuwata, M., Thota, A., Sumin, S., Butt, E.,
516 Wiedinmyer, C., and Spracklen, D.: Population exposure to hazardous air quality due to the 2015 fires in
517 Equatorial Asia, *Scientific reports*, 6, 1-9, 2016.

518

519 Dennis, R. A., Mayer, J., Applegate, G., Chokkalingam, U., Colfer, C. J. P., Kurniawan, I., Lachowski, H., Maus,
520 P., Permana, R. P., and Ruchiat, Y.: Fire, people and pixels: linking social science and remote sensing to
521 understand underlying causes and impacts of fires in Indonesia, *Human Ecology*, 33, 465-504, 2005.

522

523 DGCC: Emission Reduction Report, Directorate General of Climate Change, 2019.

524

525 Falk, D. A., Miller, C., McKenzie, D., and Black, A. E.: Cross-scale analysis of fire regimes, *Ecosystems*, 10,
526 809-823, 2007.

527

528 Fanin, T., and Werf, G. R.: Precipitation–fire linkages in Indonesia (1997–2015), *Biogeosciences*, 14, 3995-4008,
529 2017.

530

531 Field, R. D., van der Werf, G. R., and Shen, S. S.: Human amplification of drought-induced biomass burning in
532 Indonesia since 1960, *Nature Geoscience*, 2, 185-188, 2009.

533

534 Field, R. D., Van Der Werf, G. R., Fanin, T., Fetzer, E. J., Fuller, R., Jethva, H., Levy, R., Livesey, N. J., Luo,
535 M., and Torres, O.: Indonesian fire activity and smoke pollution in 2015 show persistent nonlinear sensitivity to
536 El Niño-induced drought, *Proceedings of the National Academy of Sciences*, 113, 9204-9209, 2016.

537

538 Fletcher, K.: SENTINEL 2: ESA's Optical High-Resolution Mission for GMES Operational Services, European
539 Space Agency, 2012.



- 539
540 Gaveau, D., Salim, M., Hergoualc'h, K., Locatelli, B., Sloan, S., Wooster, M., Marlier, M., Molidena, E., Yaem, H.,
541 DeFries, R., Verchot, L., Murdiyarso, D., Nasi, R., Holmgren, P. & Sheil, D.: Major atmospheric emissions from peat
542 fires in Southeast Asia during non-drought years: evidence from the 2013 Sumatran fires. *Scientific Reports*
543 4:6112, 2014.
544
545 Gaveau, D. L., Pirard, R., Salim, M. A., Tonoto, P., Parks, S. A., and Carmenta, R.: Overlapping land claims limit
546 the use of satellites to monitor No-Deforestation commitments and No-Burning compliance, *Conservation Letters*,
547 2017.
548
549 Giglio, L., Boschetti, L., Roy, D. P., Humber, M. L., and Justice, C. O.: The Collection 6 MODIS burned area
550 mapping algorithm and product, *Remote sensing of environment*, 217, 72-85, 2018.
551
552 Gorelick, N., Hancher, M., Dixon, M., Ilyushchenko, S., Thau, D., and Moore, R.: Google Earth Engine:
553 Planetary-scale geospatial analysis for everyone, *Remote Sensing of Environment*, 202, 18-27, 2017.
554
555 Huang, H., Roy, D. P., Boschetti, L., Zhang, H. K., Yan, L., Kumar, S. S., Gomez-Dans, J., and Li, J.: Separability
556 analysis of Sentinel-2A Multi-Spectral Instrument (MSI) data for burned area discrimination, *Remote Sensing*, 8,
557 873, 2016.
558
559 Huijnen, V., Wooster, M., Kaiser, J., Gaveau, D., Flemming, J., Parrington, M., Inness, A., Murdiyarso, D., Main,
560 B., and Van Weele, M.: Fire carbon emissions over maritime southeast Asia in 2015 largest since 1997, *Scientific*
561 *reports*, 6, 26886, 2016.
562
563 Karsai, I., Schmickl, T., and Kampis, G.: Forest Fires: Fire Management and the Power Law, in: *Resilience and*
564 *Stability of Ecological and Social Systems*, Springer, 63-77, 2020.
565
566 Key, C. H., and Benson, N. C.: The Normalized Burn Ratio (NBR): A Landsat TM radiometric measure of burn
567 severity, United States Geological Survey, Northern Rocky Mountain Science Center.(Bozeman, MT), 1999.
568
569 Koplitz, S., Mickley, L., Jacob, D., Marlier, M. E., DeFries, R., Gaveau, D. L., Locatelli, B., Reid, J., Xian, P.,
570 and Myers, S.: Role of the Madden-Julian Oscillation in the Transport of Smoke From Sumatra to the Malay
571 Peninsula During Severe Non-El Niño Haze Events, *Journal of Geophysical Research: Atmospheres*, 123, 6282-
572 6294, 2018.
573
574 Koplitz, S. N., Mickley, L. J., Marlier, M. E., Buonocore, J. J., Kim, P. S., Liu, T., Sulprizio, M. P., DeFries, R.
575 S., Jacob, D. J., and Schwartz, J.: Public health impacts of the severe haze in Equatorial Asia in September–
576 October 2015: demonstration of a new framework for informing fire management strategies to reduce downwind
577 smoke exposure, *Environmental Research Letters*, 11, 094023, 2016.
578
579 Kurniadi, A., Weller, E., Min, S.-K., and Seong, M.-G.: Independent ENSO and IOD impacts on rainfall extremes
580 over Indonesia, *International Journal of Climatology*, n/a, <https://doi.org/10.1002/joc.7040>, 2021.
581
582 Liu, S., Zheng, Y., Dalponte, M., and Tong, X.: A novel fire index-based burned area change detection approach
583 using Landsat-8 OLI data, *European journal of remote sensing*, 53, 104-112, 2020.
584
585 Lohberger, S., Stängel, M., Atwood, E. C., and Siegert, F.: Spatial evaluation of Indonesia's 2015 fire-affected
586 area and estimated carbon emissions using Sentinel-1, *Global change biology*, 24, 644-654, 2018.
587
588 Malamud, B. D., Morein, G., and Turcotte, D. L.: Forest fires: an example of self-organized critical behavior,
589 *Science*, 281, 1840-1842, 1998.
590
591 Miettinen, J., Shi, C., and Liew, S. C.: Fire distribution in Peninsular Malaysia, Sumatra and Borneo in 2015 with
592 special emphasis on peatland fires, *Environmental management*, 60, 747-757, 2017.
593
594 Nikonovas, T., Spessa, A., Doerr, S. H., Clay, G. D., and Mezbahuddin, S.: Near-complete loss of fire-resistant
595 primary tropical forest cover in Sumatra and Kalimantan, *Communications Earth & Environment*, 1, 1-8, 2020.
596
597 Olofsson, P., Foody, G. M., Herold, M., Stehman, S. V., Woodcock, C. E., and Wulder, M. A.: Good practices
598 for estimating area and assessing accuracy of land change, *Remote Sensing of Environment*, 148, 42-57,
599 <http://dx.doi.org/10.1016/j.rse.2014.02.015>, 2014.
600



- 601 Ritung, S., Wahyunto, Nugroho, K., Sukarman, Hikmatullah, Suparto, and C, T.: Peatland map of Indonesia,
602 Department of Research and Development of Agricultural Land Resources, Ministry of Agriculture, 2011.
603
604 Rochmyaningsih, D.: Wildfire researcher deported amid growing rift between Indonesian government and
605 scientists, *Science*, 367, 722-723, 2020.
606
607 Recapitulation of Land and Forest Fires Area (Ha) per Province in Indonesia 2015-2020:
608 http://sipongi.menlhk.go.id/hotspot/luas_kebakaran, 2020.
609
610 Sloan, S., Locatelli, B., Wooster, M. J., and Gaveau, D. L.: Fire activity in Borneo driven by industrial land
611 conversion and drought during El Niño periods, 1982–2010, *Global environmental change*, 47, 95-109, 2017.
612 Sloan, S., Tacconi, L., and Cattau, M.: Fire prevention: Successes and limitations in Indonesia, *Mitigation and*
613 *Adaptation Strategies for Global Change*, Under Review.
614
615 Stehman, S. V., Wickham, J., Smith, J., and Yang, L.: Thematic accuracy of the 1992 National Land-Cover Data
616 for the eastern United States: Statistical methodology and regional results, *Remote Sensing of Environment*, 86,
617 500-516, 2003.
618
619 Tansey, K., Beston, J., Hoscilo, A., Page, S., and Paredes Hernández, C.: Relationship between MODIS fire hot
620 spot count and burned area in a degraded tropical peat swamp forest in Central Kalimantan, Indonesia, *Journal of*
621 *Geophysical Research: Atmospheres*, 113, 2008.
622
623 van Nieuwstadt, M. G. L., and Sheil, D.: Drought, fire and tree survival in a Borneo rain forest, East Kalimantan,
624 Indonesia, *Journal of Ecology*, 93, 191-201, 2005.
625
626 Wooster, M., Gaveau, D., Salim, M., Zhang, T., Xu, W., Green, D., Huijnen, V., Murdiyarso, D., Gunawan, D.,
627 and Borchard, N.: New tropical peatland gas and particulate emissions factors indicate 2015 Indonesian fires
628 released far more particulate matter (but less methane) than current inventories imply, *Remote Sensing*, 10, 495,
629 2018.

630

631

632

633

634

635

636

637

638

639

640

641

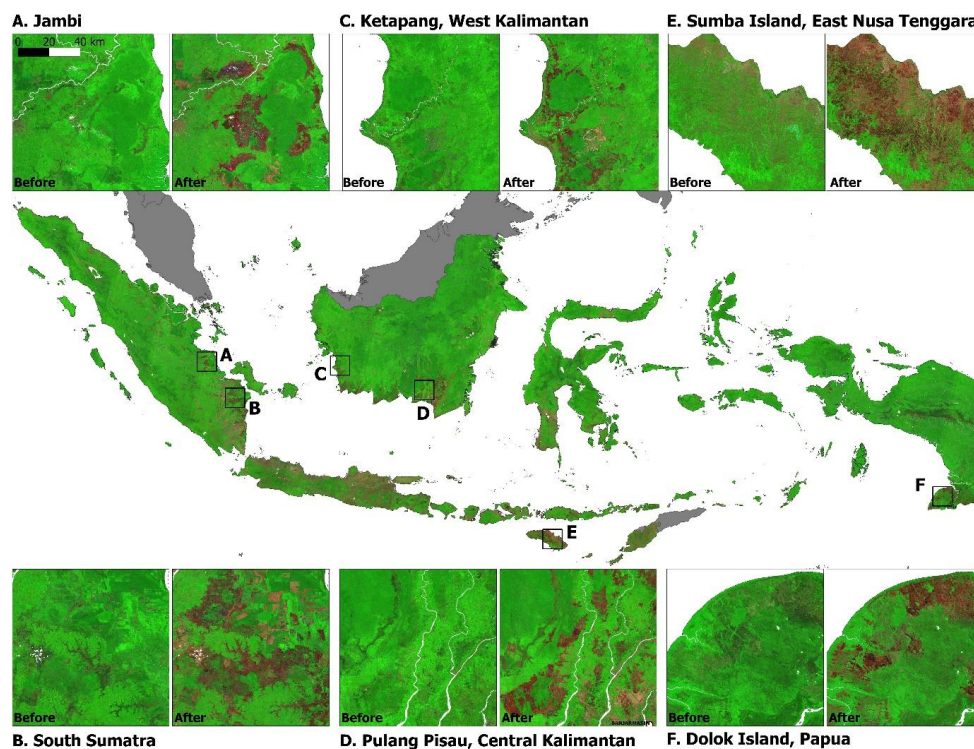
642

643 **Figures**

644



645



646

647 **Figure 1.** The pair of cloud-free pre-and post-fire Sentinel-2 composites shown over six locations in insets A, B, C, D, E, F
648 (all insets have the same scale). The base Indonesia-wide imagery is the post-fire composite. Imagery displayed in false colors
649 (RGB: short-wave infrared (band 11); Near infrared (band 8), Blue: red (band 4)). In this pair of composite images acquired
650 shortly before and after fire a recently burned area will readily appear to have transitioned from 'green' to dark 'brown/red'
651 tones. Areas cleared without burning appear bright pink. Areas covered with vegetation appear dark to bright green.
652

653

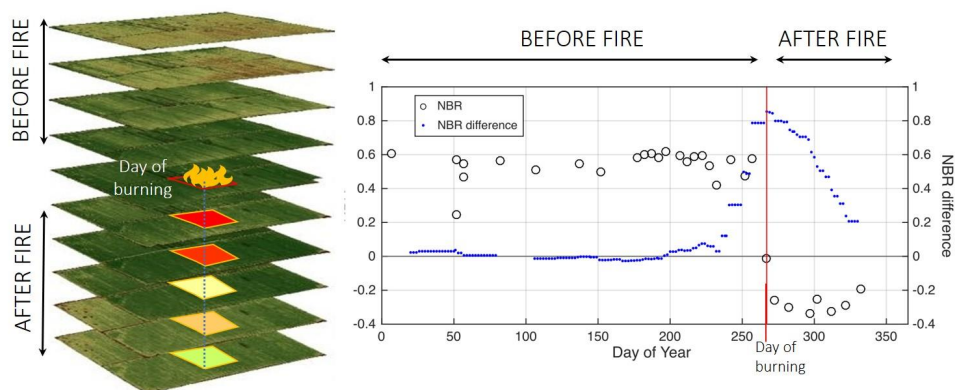
654

655

656

657

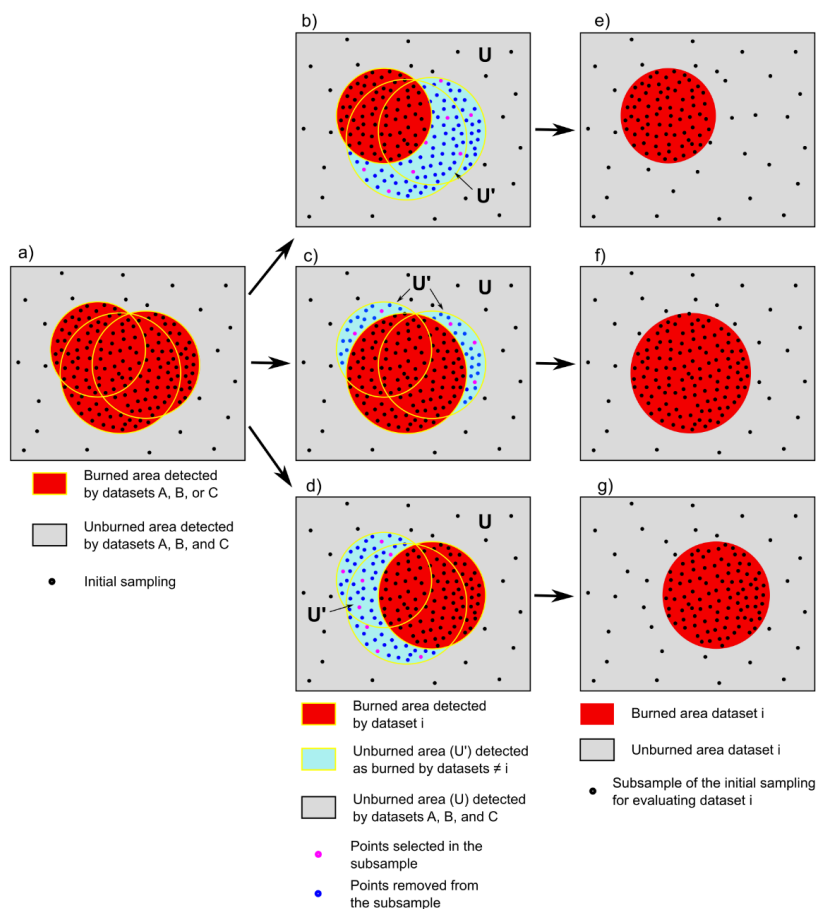
658



659

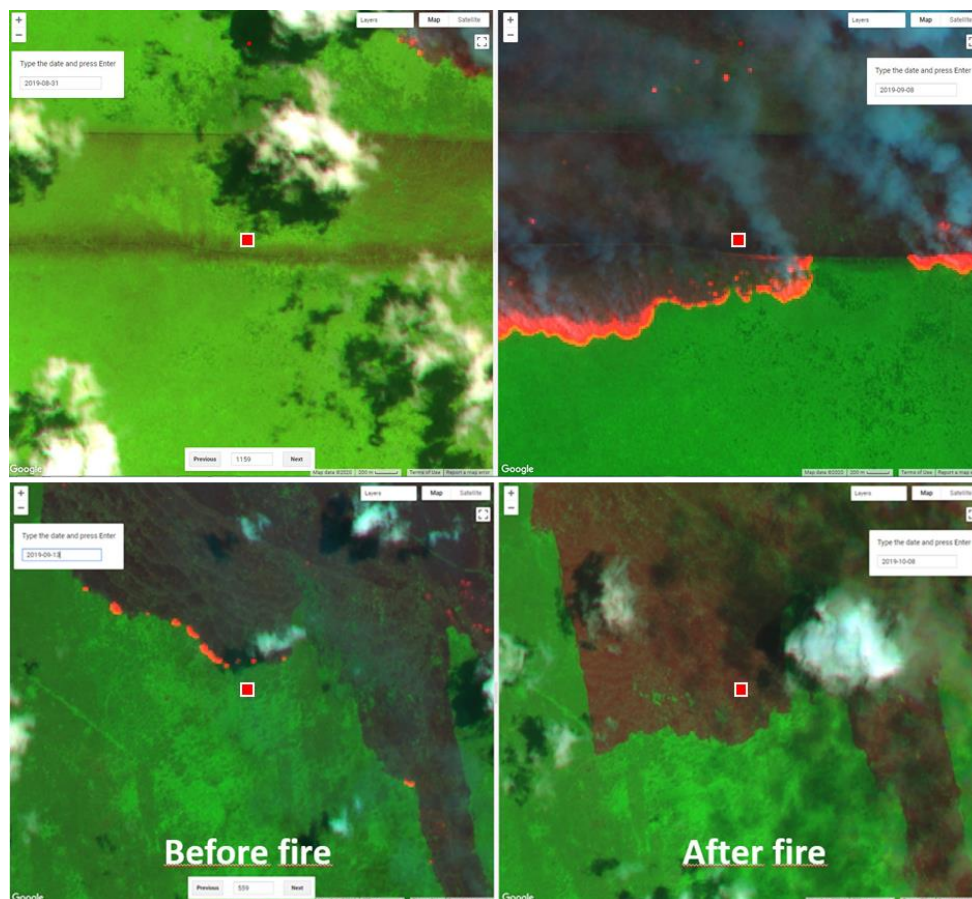
660 **Figure 2.** A schematic of Sentinel-2 time-series imagery, associated NBR values (open circles) and NBR differences between
661 average NBR values observed before and after the central day of a 2-day moving window (blue dots). A burned pixel (20 m x
662 20 m) is represented by a red rectangle at left. Before fire, the vegetated pixel registers positive NBR values (open circles).
663 The NBR rapidly drops during the fire and, for a few weeks, the satellite observations show a negative NBR. The day of the
664 year when the NBR difference observed via the moving window reaches a maximum corresponds to the moment NBR dropped
665 (red line). This day marks a decline in the pixel's vegetation, possibly reflecting a burning event. Over time, the vegetation
666 regenerates (re-greening) and the spectral characteristic of charred vegetation fades. Regreening can happen within days in the
667 case of savanna grasslands, or within months in the case of forest fires on peatlands.

668
669
670
671



672

673 **Figure 3.** Representation of the adjusted, stratified-sampling design for the validation of three burned area datasets (A, B, and
 674 C) against reference sites (dots). Panel (a) shows the stratified random sampling of reference sites (black points) over the
 675 combined burned area. Note that the density of samples is higher in the combined burned area than the unburned area. Panels
 676 (b), (c), and (d) show, in cyan, the area U' , being classified as unburned in a given dataset i but classified as burned in at least
 677 one other datasets $\neq i$. For a given validation of A, B, and C, the sample points in the corresponding area U' (panels (b), (c),
 678 (e)) were randomly excluded until the sampling density in the area U' equaled that of the larger unburned area U (area in gray).
 679 Panels (f), (g) and (h) show the three final, adjusted, stratified subsamples of reference points derived from the initial sample
 680 of 1298 reference points. Note that the relative areas and number of sites per class in Figure 3 do not correspond to the actual
 681 datasets being evaluated.



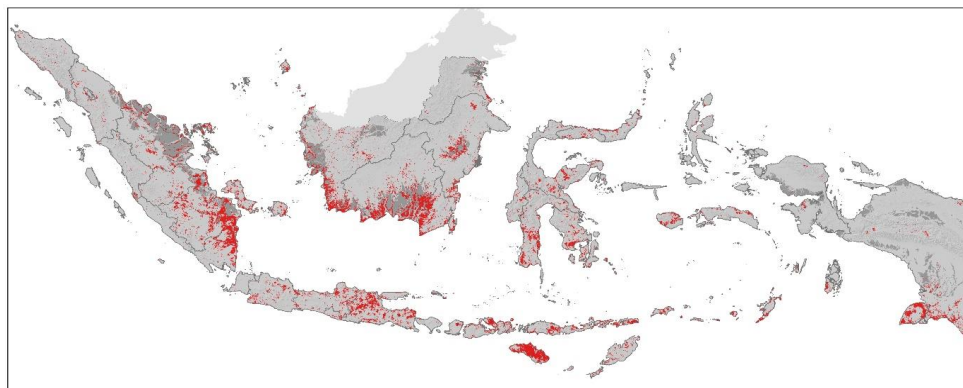
682

683 **Figure 4.** Two snapshots recording the pre-fire (left panel) and post-fire (right panel) original Sentinel-2 images acquired
684 shortly before (13 September 2019) and shortly after (08 October 2019) fire for two reference site (red squares). Imagery
685 displayed in RGB: SWIR, NIR, RED. Sentinel-2 provides two SWIR Bands. Band 12=2.190 μm is more suitable than Band
686 11=1.610 μm to detect the intense heat from flaming fronts. On these image pairs, one can see flaming fronts traveling towards
687 the reference sites (red dot) from the north on the pre fire images (left), and sharp changes in color from 'green' to 'dark red'
688 characteristic of charred remains with continuing flaming on the post-fire images (right). Layout built using © Google Earth
689 Engine.

690

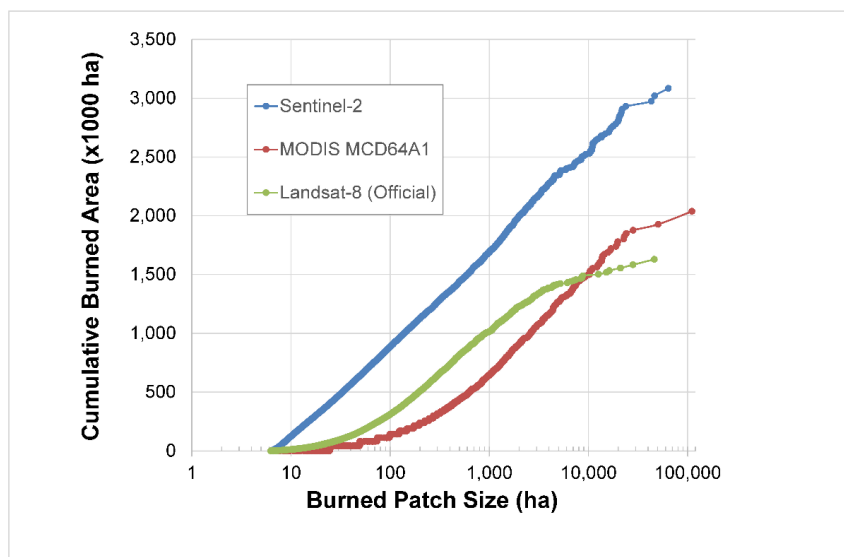
691

692



693

694 **Figure 5.** 2019 burned areas (red) for Indonesia derived using a time-series of the atmospherically corrected surface reflectance
695 multispectral images (level 2A product) taken by the Sentinel-2 A and B satellites. The spatial resolution of this map is 20 m
696 x 20 m, and Minimum mapping unit is 6.25 ha. The officially recognized peatlands extent is shown with the darkest shade of
697 grey. A provincial breakdown of burned areas according to our map estimates and those of the Official and the MCD64A1
698 product are given in Figure S1.
699



700

701 **Figure 6.** Cumulative national total burned area versus burned-scar area, for Sentinel-2, Landsat-8 (Official), and MODIS
702 MCD64a1 burned-area estimates. Scars < 6.25 ha are not shown. Note the logarithmic axis. For a given segment of the x-
703 axis between scar sizes X_1 and X_2 , a difference in the slopes for any two estimates is indicative of inter-estimate differences
704 in terms of inclusivity of scars between X_1 and X_2 .
705

706

707



708 **Tables**

709

710 **Table 1.** Adjusted, Stratified Subsamples of Reference Sites to Validate Burned-Area Estimates.

Burned-Area Estimate	Reference Sites		Total Reference Sites
	In Areas Classified as Burned	In Areas Classified as Unburned (U & U')	
Sentinel-2 (this study)	888	280	1168
MODIS MCD64A1	891	242	1133
Landsat-8 (Official)	895	182	1077

711

712 **Table 2.** Accuracy assessment of each of the three burned area maps performed in seven Indonesian provinces (87.60 Mha)
 713 targeted for peatland restoration. The accuracy metrics were estimated with an initial total of 1,298 points randomly distributed
 714 using stratified sampling. The reported metrics are: 1) the overall accuracy (OA), the user's accuracy (UA), and the producer's
 715 accuracy (PA) with their 95% confidence intervals, and 2) the mapped burned area and the corrected burned area with their
 716 95% confidence intervals.

	SENTINEL	OFFICIAL	MCD64A1
OA (%)	99.3 (99.1, 99.6)	98.1 (97.8, 98.5)	98.4 (98.1, 98.8)
UA (%)	Burned 97.9 (97.1, 98.8) Unburned 99.3 (99.1, 99.6)	95.1 (93.5, 96.7) 98.6 (98.2, 99.0)	76.0 (73.3, 78.7) 98.8 (98.5, 99.2)
PA (%)	Burned 75.6 (68.3, 83.0) Unburned 99.9 (99.9, 99.9)	49.5 (42.5, 56.6) 99.9 (99.9, 99.9)	53.1 (45.8, 60.5) 99.6 (99.6, 99.7)
Mapped burned area (Mha)	1.84	1.19	1.58
Corrected burned area (Mha)	2.38 (2.14, 2.61)	2.29 (1.96, 2.63)	2.27 (1.94, 2.59)
Difference (Mha)	0.54	1.1	0.69

717

718 **Table 3.** Tests statistics with respect to three-way differences in burned area scar-size frequency distributions for Sentinel,
 719 MODIS, and official estimates.

Scar Size (ha)	Kruskal-Wallis H ^a
> 6.25	10,478**
> 20	998*
> 100	335*
> 1000	14*
> 5000 ^a	0.61

720

721 Significance: ** p<0.0001; * p<0.001

722 Notes: Scar-size thresholds in the table denote the set of scars included in a test. Tests pertain to whether frequency
 723 distributions have equivalent 'distribution location', that is, position along a continuum of scar sizes. Tests thus pertain to
 724 whether the estimates capture distinct realms of fire activity, assuming similarly shaped frequency distributions. Higher test
 725 statistic values indicate greater probability that the estimates differ with respect to distribution location. The tree-way
 726 comparisons of the estimates may flag differences where all three estimates differ or where only two of the three differ.
 727 Significance is not Bonferroni corrected. (a) There are 56, 60 and 16 scars > 5000 ha for Sentinel, MCD64A1, Official
 728 estimates, respectively.
 729

730

731

732



733 **Table 4.** Test statistics with respect to two-way differences in burned area scar-size frequency distributions, with respect to
 734 distribution shape and situation (Test I) or situation alone (Test II), for Sentinel estimates compared to either MCD64A1 or
 735 Official estimates.
 736

Scar Size (ha)	Sentinel vs. MCD64A1		Sentinel vs. Official			
	I. Kolmogorov-Smirnov score (Most Extreme Difference [positive/negative]) ^b	Z-	II. Mann- Whitney U Z- score	I. Kolmogorov-Smirnov score (Most Extreme Difference [positive/negative]) ^b	Z-	II. Mann- Whitney U Z- score
> 6.25	46.9** (+0.69)		-82.9**	31.8** (+0.32)		-70.6**
> 20	14.7** (+0.24/0,-15)		-20.1*	13.2** (+0.18)		-28.6*
> 100	7.9** (+0.23)		-16.6*	1.6 [†] (+0.04/-0.04)		-0.57
> 1000	0.76 (+0.06/-0.03)		-0.79	1.5 [‡] (+0.01/-0.12)		-3.1*
> 5000 ^a	0.72 (+0.14/-0.08)		-0.77	0.70 (+0.13/-0.20)		0.10

737 Significance: ** p<0.0001; * p<0.001; • p<0.01; † p=0.014; ‡ p<0.05
 738 Notes: Scar-size thresholds denote the cohort of scars included in a test. Test I and Test II both pertain to whether the Sentinel
 739 estimates capture distinct realms (scar-size cohorts) of fire activity compared to the other two estimates. Test I pertains to
 740 whether the scar-size frequency distribution of the Sentinel estimate has the same shape and ‘distribution location’ as either
 741 the MODIS or official estimate. Test II is the same but with respect to distribution location only. Distribution location refers
 742 to the situation of a frequency distribution along a continuum of scar sizes. Higher test statistics indicate greater probability
 743 that the estimates differ significantly with respect to distribution shape and/or location. Reported statistical significance is
 744 without Bonferroni corrections. a) There are 56, 60 and 16 scars > 5000 ha for Sentinel, MODIS, official estimates,
 745 respectively. (b) Largest positive and negative differences in the cumulative probability functions of Sentinel vs. MODIS or
 746 official scar-size estimates. No difference was reported where it was <0.00 absolutely.
 747
 748